

# Perspective on petahertz electronics and attosecond nanoscopy

J. Schoetz,<sup>1,2</sup> Z. Wang,<sup>1,2</sup> E. Pisanty,<sup>3</sup> M. Lewenstein,<sup>3,4</sup> M. F. Kling,<sup>1,2,\*</sup> and M. F. Ciappina<sup>5,†</sup>

<sup>1</sup>Max Planck Institute for Quantum Optics, D-85748, Garching, Germany

<sup>2</sup>Physics Department, Ludwig-Maximilians-Universität Munich, D-85748, Garching, Germany

<sup>3</sup>ICFO - Institut de Ciències Fotoniques, The Barcelona Institute of Science and Technology, 08860 Castelldefels (Barcelona), Spain

<sup>4</sup>ICREA, Passeig Lluís Companys 23, 08010 Barcelona, Spain

<sup>5</sup>Institute of Physics of the ASCR, ELI-Beamlines, Na Slovance 2, 182 21, Prague, Czech Republic

(Dated: 11 November 2019)

The field of attosecond nanophysics, combining the research areas of attosecond physics with nanoscale physics, has experienced a considerable rise in recent years both experimentally and theoretically. Its foundation rests on the sub-cycle manipulation and sampling of the coupled electron and near-field dynamics on the nanoscale. Attosecond nanophysics not only addresses questions of strong fundamental interest in strong-field light-matter interactions at the nanoscale, but also could eventually lead to a considerable number of applications in ultrafast, petahertz-scale electronics, and ultrafast metrology for microscopy or nanoscopy. In this perspective, we outline the current frontiers, challenges, and future directions in the field, with particular emphasis on the development of petahertz electronics and attosecond nanoscopy.

This document is the unedited Author's version of a Submitted Work that was subsequently accepted for publication in ACS Photonics, copyright © American Chemical Society after peer review. The final edited and published work is available as [ACS Photonics 6, 12, 3057-3069 \(2019\)](#).

Ultrafast electronic dynamics of solid-state materials, particularly under light excitation, are of great interests both fundamentally and practically due to the wide applications of optoelectronic devices, such as transistors, photovoltaics, or photodetectors. While conventional semiconductor-based optoelectronic devices are operated based on the light intensity, lightwave-based petahertz electronics describe the manipulation of charge carrier dynamics by the electromagnetic field of light owing to the precisely controlled carrier-envelope phase (CEP) in few-cycle laser pulses at few and sub-femtosecond time scales [1, 2]. The driven ultrafast electronic dynamics, induced by intense few-cycle pulses, could occur at time scales of 10–1000 attoseconds ( $1\text{as} = 10^{-18}\text{s}$ ) [3–5]. For instance, attosecond light pulses can be created in gases as a result of the highly nonlinear high-harmonic generation (HHG) process, where electron photoionization of gas atoms is restricted to a time window much shorter than a half-cycle of the oscillation of the driving laser light field, typically on the order of sub-100 as for optical frequencies [6, 7]. While the lightwave-induced strong-field processes in gas-phase atoms and molecules have been under intensive investigations, leading to the birth of attosecond physics (see e.g. [3, 8–14]), the exploration of lightwave-driven petahertz electronics in condensed matter at conditions of extreme nonlinearity is still in its early phase and has become an emerging field of research. Lightwave electronics in solids, i.e. dielectrics, semiconductors and metals, involves characteristically different and richer electronic dynamical processes due to their complex band-structure [15]. Current research monitors light-field driven electron motions in solids mostly through either optical signal detection, e.g. HHG [16–21] or pump-probe experiments [22, 23]; detection of the emitted electrons [24]; or light-induced current sampling [25–28]. Moreover, there are even proposals to detect topological order in topological insulators [29–31]

or properties of strongly correlated electrons in solids [32] using HHG. With the ability to control electronic dynamics in solids on attosecond time scales, the development of lightwave electronics holds promise for realizing ultrafast signal processing devices at frequencies up to the petahertz regime ( $1\text{PHz} = 10^{15}\text{Hz}$ ) [1].

The development of light-driven petahertz electronics is inherently connected to solid state nanophysics in two ways. First, the natural length scale of electron motion on the few attosecond time scale is on the order of

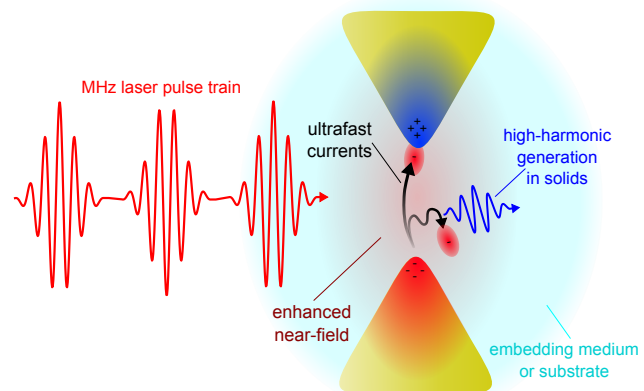


FIG. 1. Lightwave-induced attosecond electron dynamics at nanostructures: An incident laser pulse induces enhanced nanoscale near-fields around the apices of the nanostructures, which can trigger ultrafast currents as well as highharmonic generation. Ultrafast current can originate from photoemission either directly from the nanostructures or from the valence band of the embedding medium. Moreover a nonlinear polarization of the medium can also induce a current between the nanostructures. High-harmonic generation in the medium occurs when the electrons are transferred to the conduction band and strongly accelerated by the driving laser pulse, either when they experience the non-parabolicity of the conduction band or by subsequent recombination with the parent hole. Both processes promise interesting applications and are used as a tool in attosecond metrology on the nanoscale.

\* [matthias.kling@lmu.de](mailto:matthias.kling@lmu.de)

† [marcelo.ciappina@eli-beams.eu](mailto:marcelo.ciappina@eli-beams.eu)

one nanometer. Second, for the development of petahertz integrated circuits, the devices have to be both on nanometer length scales and be based on non-resistive processes, such as ballistic electron transport. Nanomaterials or nanostructured solids provide an excellent basis for the development of lightwave-driven electronics. Specifically, nanomaterials with tailored structure at extremely small scale possess unique electronic properties that can hardly be seen in bulk materials; for example, the strong quantum confinement effects and the greatly enhanced non-trivial quantum properties of semiconducting nanowires [33–35], quantum dots and semiconductor arrays [36–38], two dimensional materials [39, 40], topological insulators [41, 42], etc. Meanwhile, the strongly enhanced local electric field and its spatial inhomogeneity, through plasmonic effects or scattering, with the presence of artificial nanostructures dramatically modify the behavior of light-matter interactions, resulting in peculiar field-driven electronic dynamics at nanometer spatial scales (for recent reviews see Refs. [43, 44]). As schematically shown in Fig. 1, the enhanced local field at the nanostructures is strong enough to induce nonperturbative nonlinear processes in the material, such as HHG in solids or electron emissions either from the nanostructures or from surrounding atoms, which could be subsequently driven by the lightwave and measured as electric current in the nano-circuit or collected by a separate electron detector or spectrometer. The exploration of the interaction between extremely short laser pulses with down to attosecond durations and nanomaterials or nanostructured solids, which has been termed attosecond nanophysics, has strong implications not only in petahertz electronics development, but also in achieving supreme space- and time resolutions in microscopy; for instance, attosecond near-field sampling has been demonstrated for sampling and reconstructing nanoscale near-field distributions on attosecond timescales [45]. Attosecond nanophysics poses a tremendous theoretical challenge in terms of modeling electronic dynamics as a result of quantum confinement effects in the material and the associated strong field processes induced by the near-field. Particularly, the treatment of spatially inhomogeneous field-driven processes needs to take into account the higher multipole orders of photon-electron coupling terms [44, 46–48]. The field of light structured beams is developing rapidly recently. Such laser beams have topological properties themselves involving the light orbital momentum and polarization (cf. [49, 50]). HHG with structured beams has very special properties [51–54] that open plethora of possible applications. Combining the structured light beams with atto-nanophysics is thus especially challenging.

Studies of attosecond physics on the nanoscale were initiated more than a decade ago with the demonstration of strong-field effects on nanostructures, such as laser-triggered field emission from nanotips [55–58] and the demonstration of strong-field photoemission induced by laser irradiation [59–61]. It has been shown that the highly nonlinear tunnelling photoemission process of metallic nanotips or nanostructures and thus emitted individual electron bursts can be finely tuned by changing the CEP of the incident few-cycle laser pulse on the attosecond time scale [62–64]. Several applications have been, therefore, derived from these studies including ultrafast microscopy [65–68], ultrafast light-driven electron-

ics such as light-driven diodes [69], and metrology for reconstruction of propagating light properties, including the CEP of few-cycle pulses [70].

Recent research has provided new opportunities for the development of petahertz electronics and attosecond nanoscopy. For example, HHG can be seen in emerging two dimensional materials [71, 72] and in different artificial nanostructures [73, 74]; ultrafast light-field driven currents, as can be seen in bulk dielectrics or wide bandgap materials, has also been measured in monolayer graphene [75]. In addition, the development of HHG by MHz-repetition rate lasers makes attosecond photoelectron emission microscopy (Atto-PEEM) possible, a technique which combines the advantages of attosecond time resolution from the attosecond streaking spectroscopy technique [76, 77] with nanometer scale spatial resolution from photoelectron microscopy [59]. Finally, ultrafast electron pulses, which in principle offer sub-nanometer resolution, is another frontier in attosecond metrology applications [78, 79]. This perspective is organized in two major parts: first, the recent development and potential of attosecond metrology for petahertz electronics applications is reviewed, which includes HHG using nanostructures as potential ultracompact XUV sources (subsection A) and ultrafast light-field induced currents in nanostructures (subsection B); Secondly, the progress, challenges, and potential of attosecond nanoscopy based on photoemission streaking spectroscopy (subsection A) and based on ultrafast electron sources (subsection B) is discussed.

## PETAHERTZ ELECTRONICS

### High-order harmonic generation with nanostructured solids and applications

Nanostructures were initially utilized for enhancing HHG in gases, which was expected to provide the potential for realizing HHG at MHz-repetition rates [81–84]. However, it has later been shown that the observed MHz-rate XUV light generated in the vicinity of nanostructures originates from incoherent atomic line emission rather than actual HHG [73, 83, 84]. The major problem here is that the effective volume, in which field enhancement takes place for HHG ( $\approx 10^{-15} \text{ mm}^3$ ), is much smaller than that in conventional HHG ( $\approx 10^{-2} \text{ mm}^3$ ). Therefore far fewer gas atoms could effectively contribute to the signal, which cannot be compensated by the increase in the repetition rate [85]. HHG in solids, which contain a much higher atomic density, could circumvent this problem.

In recent years, HHG in solids has been studied intensively [16–20]. Different from gas-based HHG, which can be well described by the classical three-step model [8], the generation mechanism of HHG in solids becomes much more complex involving inter- and intra-band electronic dynamics [86]. Therefore, the classical three-step model is no longer well-suited since both of the electron and hole dynamics within the entire Brillouin zone of the crystal need to be considered [21]. Practically, HHG in solids exhibits distinct features compared to that in gases. For instance, the HHG spectrum is sensitive to the crystal symmetry and band structure, which allows the appearance of even-order harmonic emission and permits the reconstruction of the band structure from the measured

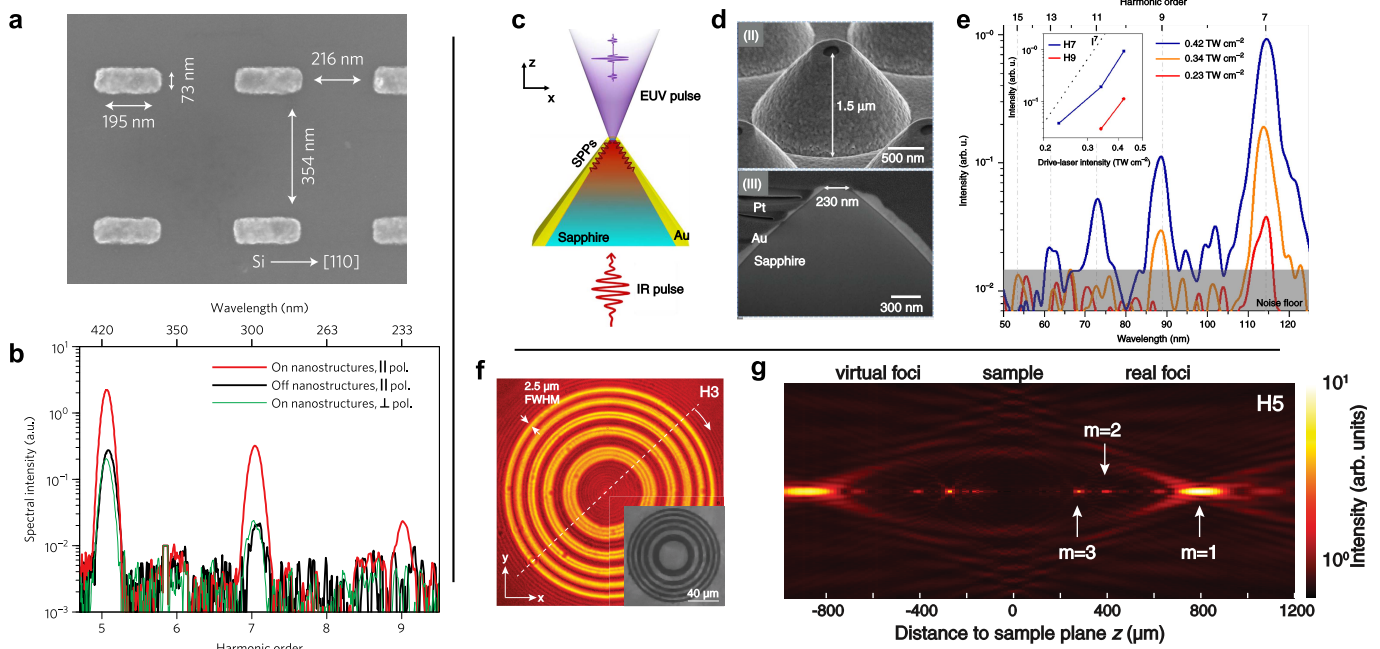


FIG. 2. High-harmonic generation in solids with nanostructures: (a) and (b) Localized surface plasmon resonance enhanced HHG with a nanoantenna array on a silicon surface [from Ref. 80]: (a) Scanning electron microscopy (SEM) image of the nanoantenna array with antenna major axis parallel to Si [110] direction. The nanoantenna array is designed with its plasmonic resonance at the center wavelength of laser excitation for HHG. (b) The measured harmonic signal, up to 9th order, is enhanced when nanoantennas are illuminated resonantly with the laser polarization parallel to the antenna major axis (red), compared to the signal when they are illuminated off-resonantly with the laser polarization perpendicular to the antenna major axis (green) and the signal from a bare Si surface (black). (c)-(e) Surface plasmon polaritons (SPPs) enhanced HHG in a metal-sapphire nanostructure [from Ref. 73]: (c) Schematic overview of the plasmonic enhanced HHG scheme: SPPs are generated and propagate along the metal-sapphire interface, and induce field enhancement close to the top of the cone, where HHG is emitted. (d) SEM image (I) and cross-section image (II) of a single cone-shape structure. (e) Measured harmonic signal at different input intensities. The inset shows the power scaling of the 7th and 9th order harmonic peaks. (f) and (g) Harmonic self-focusing from a Fresnel zone plate (FZP) pattern fabricated by gallium implantation in a silicon surface [from Ref. 74]: (f) Image of the FZP collected from its third harmonic emission at the sample position. The inset shows a SEM image of the FZP. (g) Spatial characterization of the 5th harmonic emission from the FZP, which shows three focus orders.

results. And since the bandgap of solids is much smaller than the ionization potential in noble gas atoms, HHG can be observed at lower laser pulse energies with sub- $\mu\text{J}$ -level. On the other hand, however, considering the fact that the emitted XUV radiation can be re-absorbed shortly after its creation depending on the type of crystal and emitted photon energies, in many cases, only the last few nanometers of material of a bulk sample finally contribute to the far-field radiation. Nevertheless, considerable HHG flux can be achieved due to the extremely high atomic density in solids [86–88].

High-harmonic generation in nanostructured solids has recently been demonstrated by several groups [71–73, 80, 89]. In the case of solids combined with plasmonic nanostructures, thanks to the resonantly enhanced local electric field, significant increase of HHG emission can be seen, see e.g. Fig. 2(a) and (b) [80]. A further demonstration of HHG intensity enhancement has been shown with tapered nano-waveguides, see Fig. 2(c)–(d) [73]. Here, the field enhancement at the tapered nanocone is induced by surface plasmon polaritons (SPP) propagating at the interface between the outer gold layer and inner sapphire (see panel (c)). In a different approach [74], the surface of semiconductors was tailored in different ways, either to manipulate the divergence properties of the high-order harmonic radiation, e.g. via Fresnel zone plates,

as shown in Fig. 2(f) and (g), or to use the field enhancement for HHG at lower input intensities. The focal-spot size generated by the Fresnel zone plates was almost diffraction-limited, and integrating the generation and focusing step could allow for very compact devices. Finally, HHG emission from an all-dielectric metasurface was recently demonstrated [90]. There, the interplay between a bright (radiating) and a dark (non-radiating) mode led to drastically increased HHG emission, and characteristic resonance effects. Since the field is directly enhanced in the structure itself, a larger volume can contribute to the HHG signal, an advantage that is also increasingly being used in nanostructure-enhanced perturbative (second or third) harmonic generation [91]. The ability to tailor the solid surface opens the door to design and tune the generated harmonic emission beams with desired properties, such as certain polarization states [92, 93], different orbital angular momentum (OAM) content of the harmonic radiation [94–96] by simple laser excitations and more elaborate beam-shaping schemes with structured-light for short-wavelength sources, which is currently still unavailable.

One of the main limitations, however, is that the enhanced electric field might damage both the structure itself and the solid substrate, at the laser intensities required for HHG [80, 97]. Therefore, the enhancement ef-

fects on HHG can be gradually undermined; for example, it has been reported that damage of the plasmonic nanostructure reduces the HHG yield over time by one order of magnitude [73]. The major damage mechanism at intensities below direct laser ablation, as shown by several studies, is due to the heating induced by electric field inside the nanostructure and the less efficient heat conduction within and away from the interaction region [97–99]. Therefore, careful design of the nanostructures for HHG is required by taking into account the optically-induced heating damage. To this end, the all-dielectric metasurface with low losses at optical frequencies is, in principle, promising; though optical damage could still occur [90]. The development of waveform-controlled few-cycle sources at longer wavelengths [100–104] will also help reduce optical damage for most materials, due to lower excitation photon energies and consequently suppressed multiphoton excitation and ionization processes [21].

The development of HHG in solids, particularly with nanostructures, is expected to lead to the realization of the next generation of ultracompact XUV light sources, which could be applied to, e.g., scanning attosecond microscopy, with up to MHz repetition rates obtained directly from the unamplified femtosecond pulses of laser oscillators.

### Ultrafast currents from nanostructures and applications

Light-field induced currents can be measured in strong-field photoemission from metallic nanostructures and in solid-state materials, particularly dielectric materials and it is the combination of both that will form the foundation of light-driven petahertz electronics. Strong-field photoemission from nanostructures, such as nanotips [55–58] and nanofilms [107–109], have been studied for over a decade. The control of electron emission on attosecond time scales, by tuning the CEP of few-cycle pulses was first discussed in 2007 and has been studied intensively ever since [59, 62–64]. It has been shown that the energy-resolved spectra of photo-emitted electrons in the regime close to the cutoff energy are strongly modulated by the CEP, which can be used to retrieve the position-resolved absolute phase of a laser beam [70]. More recently, experiments have shown that the total electron yield from a single junction [105] or from an array of nanostructures [106] is also CEP dependent, see Fig. 3. The control of current flowing across the junctions by the laser pulse's CEP carries great potential in ultrafast current switching for the realization of petahertz electronics. Moreover, the fact that these experiments were performed under ambient conditions without any vacuum apparatus opens up more general applications.

The discovery of controlled ultrafast currents in dielectrics has evoked substantial interest in recent years [25–28]. The attosecond response of dielectrics and wide-bandgap semiconductors, even without resonant photo-excitation of interband transitions, primarily results from light-induced strong-field effects, which permit unprecedentedly fast electronic switching at optical frequencies (PHz) with low heat dissipation [1]. The studies of petahertz electronics and related devices are still in an

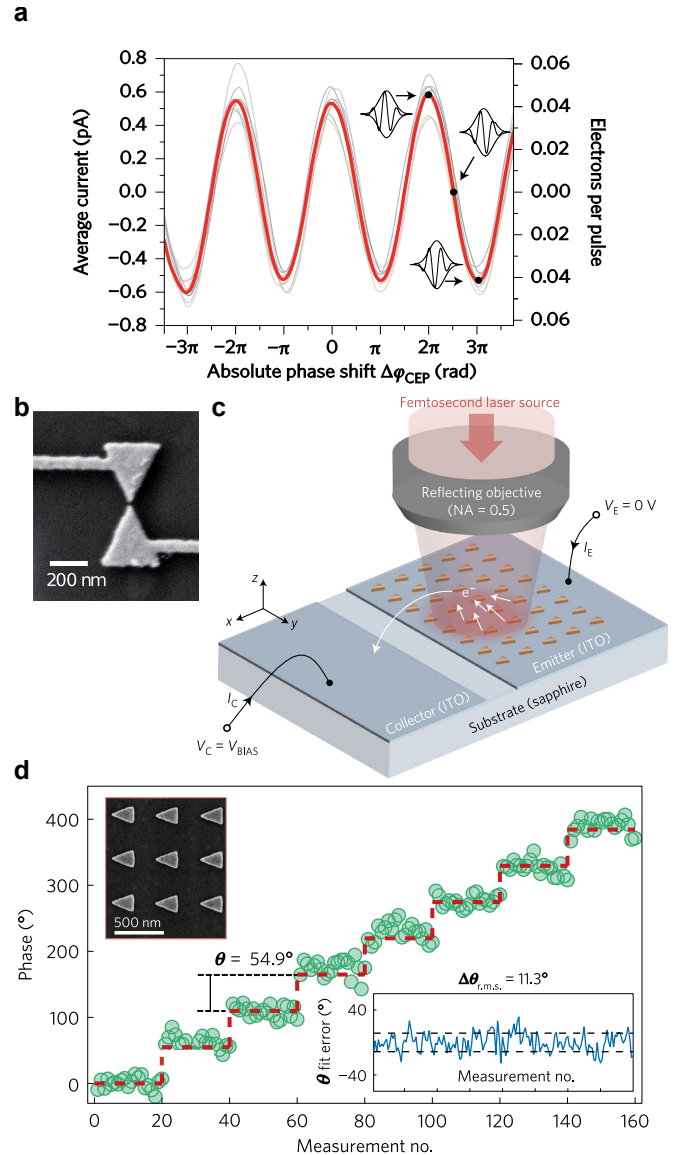


FIG. 3. Electric field sensitive ultrafast currents from nanostructures: (a) and (b) CEP-controlled tunneling current through a single bow-tie nanogap [from Ref. 105]: (a) Average current (red line) measured through a bowtie nanostructure dependent on the CEP of the few-cycle laser pulse. The waveform of the laser pulse at three different CEPs is also shown. (b) SEM image of the bow-tie structure. (c) and (d) CEP-dependent photoemission current from a nanostructure array [from Ref. 106]: (c) Schematic experimental setup. A few-cycle laser pulse is focused onto a nanostructure array. Photoemitted electrons are collected by the ITO collector across a micrometer-size gap under a positive bias voltage. (c) Stepwise changes in the source's CEP result in stepwise changes in the phase of the current detected by a lock-in amplifier. The upper inset shows a SEM image of the structure. The lower inset shows the deviation of measured phase of the electron current with respect to the CEP set value of the laser pulse.

early phase. Light-driven electronic devices fabricated from dielectrics materials, such as fused silica ( $\text{SiO}_2$ ) [25], quartz, sapphire [110], calcium fluoride ( $\text{CaF}_2$ ) [111], and wide-bandgap semiconductors, such as gallium nitride ( $\text{GaN}$ ) [28], exhibit CEP-dependent photocurrent induced by few-cycle laser pulses. As one of the appli-

cations, a solid-state light phase detector that is able to measure the absolute CEP of few-cycle laser fields has been demonstrated [27]. Other types of devices, for instance, the petahertz diode [112] and optical memory devices [113] have been theoretically proposed, however, have not yet been realized. In the meantime, attosecond spectroscopy measurements on these materials has revealed the strong light field induced electronic dynamics at frequencies up to multi-PHz [26, 114–116].

There are several challenges that need to be overcome. First, the field-dependent signals in currents from nanostructures, that have been demonstrated so far, are rather weak, on the order of  $10^{-4}$  of the total signal [106] and the single-shot field-dependent measurement has not yet been realized, while the potential limitations of space-charge effects are still not well understood. Furthermore, miniaturization of ultrafast current switches down to the few nanometer scale, which means short distances between gates, seems to be not only beneficial in terms of integrated devices, but is also necessary to fully exploit the speed-up in switching rate by avoiding communication delays. Such a down-scaling ultimately requires to overcome the diffraction limit and is still to be demonstrated. Moreover, for an implementation of PHz electronics, an increase of clock rate from the currently-demonstrated switches employing kHz sources is required. However, controlled few-cycle light waveforms are, so far, only available with MHz-rate, and a further increase in repetition rate would demand corresponding developments in femtosecond laser technology. Finally, similar to nanostructure-enhanced HHG, optically induced damage mainly due to heat deposition, is expected to be one of the major obstacles. Therefore, the creation of strong electric fields with low energy input pulses is necessary.

In order to down-scale the devices and to couple the exciting light into the nanoscale devices, nanoplasmonic systems, which confine electromagnetic energy down to sub-wavelength length scales, seem to be very promising. Near-field enhancement moreover reduces effectively the required input laser pulse energies. Adiabatic nanofocusing of few-cycle light pulses [117] is one of the potential building blocks, where a few-cycle pulse can efficiently be coupled to the SPP of a sharp metallic nanotip, allowing to confine electromagnetic fields down to the nanometer scale with giant near-field intensities [118–121]. Under the same nanotip geometry, the lightwave-controllable ultrafast current source from strong-field photoemission of nanostructures, as discussed above [105, 106], may also play a role so that a combination of these two elements can be designed to scale the entire circuitry down to the nanometer scale. One possible route towards THz repetition rate few-cycle light waveforms, would be the use of mode-locked quantum cascade lasers [122–124] or solitons in microresonators [125–127], which currently provide repetition rates from GHz up to several THz. Their development is also fueled by possible applications in frequency comb spectroscopy [128, 129]. Since a laser source with such high repetition rate ( $f_{rep}$ ) requires a small resonator length ( $L = c/f_{rep}$ , where  $c$  is the speed of light), and integrated on-chip high repetition rate laser sources have been demonstrated [130].

We think that all building blocks for PHz integrated electronics would be available and we believe that bringing them together has the potential to revolutionize elec-

tronics.

## ATTOSECOND NANOSCOPY

### Attosecond photoemission electron microscopy

The principle of the attosecond-resolved photoemission electron microscope (Atto-PEEM) is shown in Fig. 4(a). A laser pulse with a properly selected central wavelength (optical light field in the range from UV to NIR) is used to photoexcite collective oscillations in nanoplasmonic structures; A co-propagating isolated attosecond XUV pulse hits the same nanostructures with a certain time delay  $\Delta t$ . Photoemitted electrons induced by the XUV pulse are spatially imaged by the energy-resolved time-of-flight photoemission electron microscope allowing nanometer spatial resolution. Since the recorded electron energy depends on the localized near-field around the nanostructure from the time of photoemission, the delay dependent electron energy spectrum reveals the dynamics of the local plasmonic field oscillations driven by the incident optical light field [59, 139]. In this way, both attosecond temporal resolution and nanometer spatial resolution can be achieved and attosecond nanoscopy realized.

Theoretical studies have shown that, since the photoemitted electrons from nanostructures can escape the near-field within an optical cycle, the recorded electron energy distribution in this case directly probes the electric near-field (the ‘instantaneous regime’) [59, 140–146]. This is in contrast to the conventional attosecond streaking spectroscopy technique, where photoionized electrons from gases experience a quasi-homogeneous field of the NIR pulse and probe the vector potential of the optical light field (the ‘ponderomotive regime’) [147]. These two regimes can be characterized by an adiabaticity parameter  $\delta = T_{esc}/T_{opt}$ , where  $T_{opt}$  is the optical period and  $T_{esc}$  is the escape time of the electron [148]. Therefore, the interpretation of streaking traces of nanoscopic near-fields requires some prior knowledge of the spatial scale of the near-field itself. Experimentally, only one study has so far demonstrated the reconstruction of nanoscale near-fields of a tapered gold nanotip [45], which, however, lacked the direct spatial resolution. Therefore, extensive numerical simulations of the electric field distributions around the nanostructure were still necessary to interpret the results. Moreover, since the focal spot of the XUV is usually much larger ( $\sim \mu\text{m}^2$ ) than the nanoscopic region of interest, typically just the hotspot of the nanostructure ( $\sim \text{nm}^2$ ), only a small portion of the total electron yield is expected to contribute to the signal.

The Atto-PEEM technique, in principle, inherits the limitations of contemporary photoemission electron microscopy (PEEM) using XUV attosecond pulse trains from HHG of gases by kHz laser sources [131, 135]. Specifically, space-charge repulsion effects on sample surface as well as in the detector, limit the admissible number of emitted electrons per pulse and thus its spatial resolution. Fig. 4(c) shows one of the examples of gold plasmonic nanostructures images collected by time-of-flight-photoemission electron microscopy (TOF-PEEM). The XUV pulses are produced from HHG of neon gas target using a kHz repetition rate laser system. Increasing the gas pressure leads to an enhanced photon flux. With

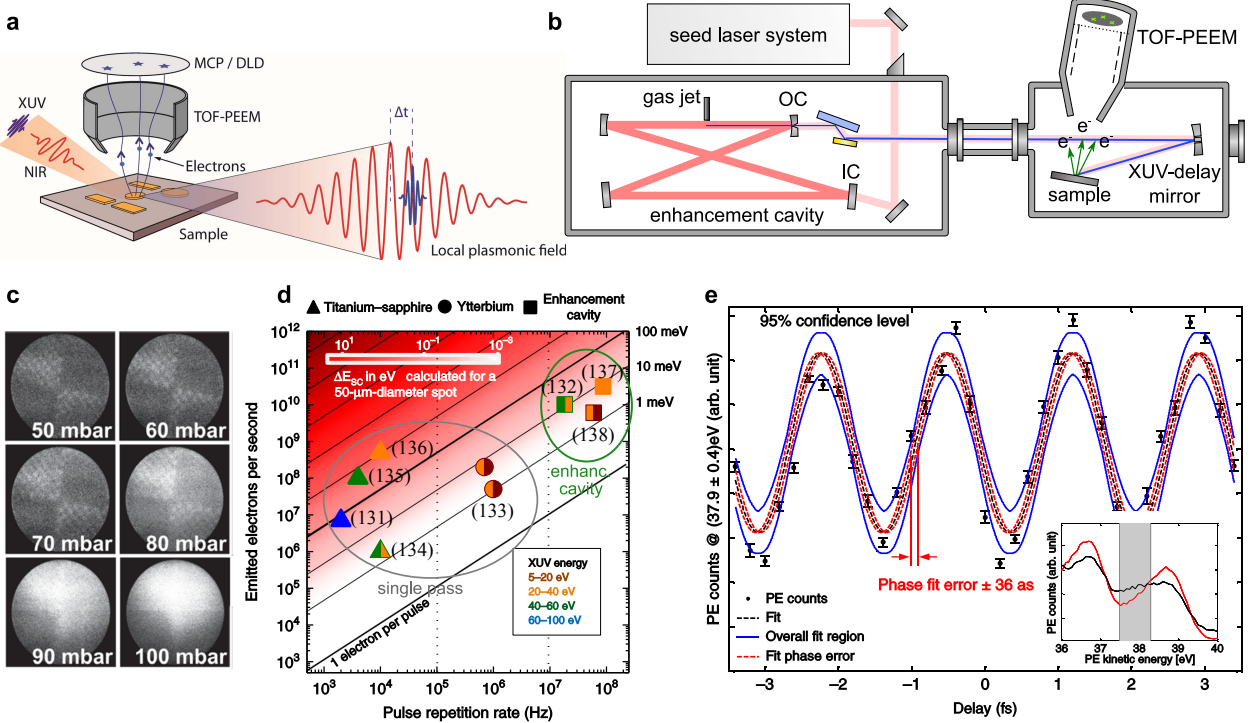


FIG. 4. Atto-PEEM and HHG in enhancement cavities: (a) Scheme of the Atto-PEEM principle [43]. A XUV laser pulse is focused onto a nanostructure and photoemits electrons, which are subsequently accelerated by the nanoplasmonic field excited by a synchronized NIR laser pulse. The final electron energy and initial position is measured using a photoelectron emission microscope. (b) Scheme of an enhancement cavity with intracavity HHG gas jet, outcoupling of the XUV radiation through a pierced mirror (OC) and time-of-flight-photoemission electron microscopy (TOF-PEEM) apparatus. (c) Example of space-charge effects limiting the photoemission microscopy imaging quality of plasmonic nanostructures [from Ref. 131]. Here, XUV pulses are generated using single-pass HHG in a neon gas target with a kHz repetition rate laser and images are collected at the same exposure time. At high XUV photon flux, i.e. gas pressures above 70 mbar, space-charge effects become observable and blur the image. (d) Comparison of HHG via single pass Ti:Sa- and Yb-based laser amplifier systems with enhancement cavities in regard to photoemission spectroscopy [from Refs. 131–138]. The color shading of the background illustrates the expected space charge broadening for a fixed spotsize. The shape and color of the symbols indicates the laser system and XUV energy range, respectively. (e) Demonstration of attosecond resolved photoemission sideband modulation on a tungsten surface from an enhancement cavity [from Ref. 132], which allows RABBITT experiments at MHz repetition rate. The red dashed lines outline phase errors of fitting results, corresponding to the time precision of the measurement of 36 as. The inset shows the photoelectron kinetic energy spectrum for two different delays between XUV and NIR laser pulse and the energy range used to determine the sideband oscillation (grey shaded region).

the same exposure time, at 70 mbar, the image become blurred due to the space-charge effects on sample surface and within the electron optics of the detector. Additionally, at 90 and 100 mbar, multiple hits on the detector create artifacts, which further reduce the image quality. Therefore, the repetition rate of kHz laser sources for HHG has become one of the major obstacles that hinders the successful implementation of Atto-PEEM: with these sources, one would need to reduce the HHG flux to levels so low that extremely long data-acquisition time (on the order of several days to a week) is necessary to reach sufficient statistics. This makes experiments impossible, since laser-stability and possible surface contamination limit the achievable acquisition time to typically just several hours.

With the development of HHG sources with MHz repetition rates, which are fueled by similar needs in conventional solid-state photoemission (e.g. [149, 150]) and XUV frequency comb spectroscopy [151], we expect that the space-charge limitation can soon be overcome. Current techniques are based on enhancement cavities [138, 151–155] or single-pass systems either using optical parametric

amplification (OPA) [156, 157] or nonlinear compression of laser pulses [158], all of which require few-cycle laser pulses with high average powers in the generation target. This is necessary since, firstly, HHG in atoms is an extremely nonlinear process which requires at least several tens of  $\mu\text{J}$  pulse energy and, secondly, conversion efficiencies from the laser pulse to the HHG radiation are small, typically in the range of  $10^{-5}$ – $10^{-6}$  [157]. Furthermore, in order to control the HHG process and generate isolated attosecond pulses, it is essential to have a tight waveform control of the laser pulses, particularly in terms of the CEP.

Enhancement cavities allow up to several kW of average power at MHz repetition rate for the generation of high-order harmonics inside the cavity. This is possible because the laser pulse is effectively reused for subsequent roundtrips. Outcoupling of the HHG radiation can either be done using pierced mirrors [132], gratings [138] or Brewster plates [153]. A schematic illustration of HHG in enhancement cavities is shown in Fig. 4(b), together with the TOF-PEEM setup. Recently, high flux XUV pulse trains with MHz repetition rate generated from an

enhancement cavity have been reported and its application to attosecond-resolved experiments on solid surface exhibits the advantage of reducing integration times from days to minutes, see Fig. 4(e) [132]. However, a central challenge still remains in this technique: so far it only delivers attosecond pulse trains, since traditional gating techniques are difficult to apply. On the one hand, the circulating laser pulses inside the cavity are usually longer than few-cycle pulses because of the limited bandwidth of the cavities [159]; on the other hand, other gating schemes designed to work with longer pulses, such as polarization gating, are hard to implement in cavity-based schemes. Nevertheless, concepts are being developed towards the generation of isolated attosecond pulses [160].

Single-pass systems can provide few-cycle pulses at only several tens to hundreds of watts in average power [157, 158]. Here, Yb-based systems have largely replaced Ti:Sapphire lasers, since they can deliver much higher average powers (albeit with lower bandwidths, which makes spectral broadening and amplification schemes necessary). In the OPA approach, a spectrally broad pulse, either from a broadband source or obtained from pulse broadening in bulk crystal, is amplified by an optical parametric process. Since the parametric process only couples to virtual energy levels in the gain material, the amplification bandwidth can be tuned by the thickness and phase-mismatch of the crystals. Moreover, the amplification process does not intrinsically require the absorption of any fraction of the photon energy in the crystal [101], therefore, the heating load can be minimized, allowing for much higher average powers than e.g. with Ti:Sa systems. Nevertheless, there is still some (regular) absorption of the interacting waves, which leads to residual heating and thermal stress and ultimately limits the achievable average power [161]. In the other approach of nonlinear compression, a high-energy laser pulse is broadened via self-phase modulation in a nonlinear medium, typically a hollow-core fibre filled with a noble gas, which is already a well-established technique in attosecond physics. Although cooling of the fibres can be necessary [162], this concept seems to allow considerably higher average powers when compared to OPA [158]. Both of these single-pass concepts allow the generation of few-cycle pulses, and they are not restricted with respect to gating schemes; indeed, the generation of HHG radiation supporting single isolated pulses at 0.6 MHz based on an optical parametric chirped-pulse amplification (OPCPA) system has been reported [163]. However, higher average power and repetition rate is still desirable for the application to Atto-PEEM. A comparison of the different HHG sources applied to photoemission in terms of emitted photoelectrons per second is shown in Fig. 4(d). At present, enhancement cavities deliver the highest space-charge limited photoelectron flux among all XUV sources thanks to their high repetition rate, while single-pass systems have the potential to catch up in the future. It will also be interesting to see if solid state HHG might become a suitable alternative.

A successful implementation of these new HHG sources will push forward the development of Atto-PEEM for attosecond nanoscopy. The new metrology techniques with the ability to measure electromagnetic fields on the attosecond temporal and nanometer spatial scale could not only allow to probe new phenomena on the nanoscale,

but ultimately benefit the development of petahertz electronics, in particular with respect to ultrafast switches or plasmonic circuitry.

### Ultrafast electron pulses and applications

The studies of strong-field electron emission from nanotips, that comprise an important pillar in attosecond nanophysics, were initially motivated by the search for new ultrafast electron sources [55], and nanotip-based electron sources are now being used in several applications, including transmission electron microscopy (TEM), ultrafast low-energy electron diffraction (ULEED) and point-projection microscopy [66, 164, 165]. Besides that, other schemes that use conventional photo-cathodes have also demonstrated ultrafast electron pulses [166]. Compared to the laser pulses, ultrafast electron pulses do not only carry the high temporal resolution but also have the advantage of possessing a high momentum at relatively low energies, which allows, in principle, for ångstrom spatial resolution. However, two disadvantages result from the use of electrons: first, Coulomb repulsion effects could be significant, when short electron pulses get focused to small spots; secondly, vacuum propagation is dispersive for electrons, which leads to an increase of the electron pulse duration as different kinetic energies travel with different speed. Therefore, the chirped electron pulses need to be simultaneously focused in space and time, which requires special and stringent compression schemes.

Practically, in order to achieve a short electron pulse duration at the sample, two different approaches have been adopted. The first approach is to minimize the distance between the source – in this case, nanotips – and the sample, so that there is a minimal increase in the electron pulse duration from the generation target to the sample; source-to-sample distances as short as 2.7  $\mu\text{m}$  have been reported [164]. In this scheme, it is important to avoid sample excitation caused by the generating laser pulse, and this can be done by nanofocusing of propagating plasmons at the tip apex, as discussed above, with the laser driver coupled to the nanotip via a grating at the shank. The other approach is to employ an additional electron pulse compression stage. The current state of the art is to use nanofoils and THz laser pulses with the electrons incident at an oblique angle, such that the electrons, depending on the timing between them and a given half-cycle of the laser field, are either accelerated or decelerated [167]. This can be used to compress or stretch the electron pulses.

If compression schemes are used, a method is needed to measure the electron pulse length and determine the optimal compression parameters. A similar arrangement as in the nanofoil compression can be used to either change the electron kinetic energy [168] or the propagation direction [166] depending on the delay between the electron and laser pulses, which allows attosecond temporal resolution. Indeed, attosecond electron pulse trains have been generated and characterized with this method [79, 169], as shown in Fig. 5(a)-(c). Attosecond electron pulse trains are generated at a nanofoil by modulating the electrons' phase via a laser pulse, which leads to sidebands in the kinetic energy spaced by multiples of the photon order. At a second nanofoil, the electrons interact with a de-

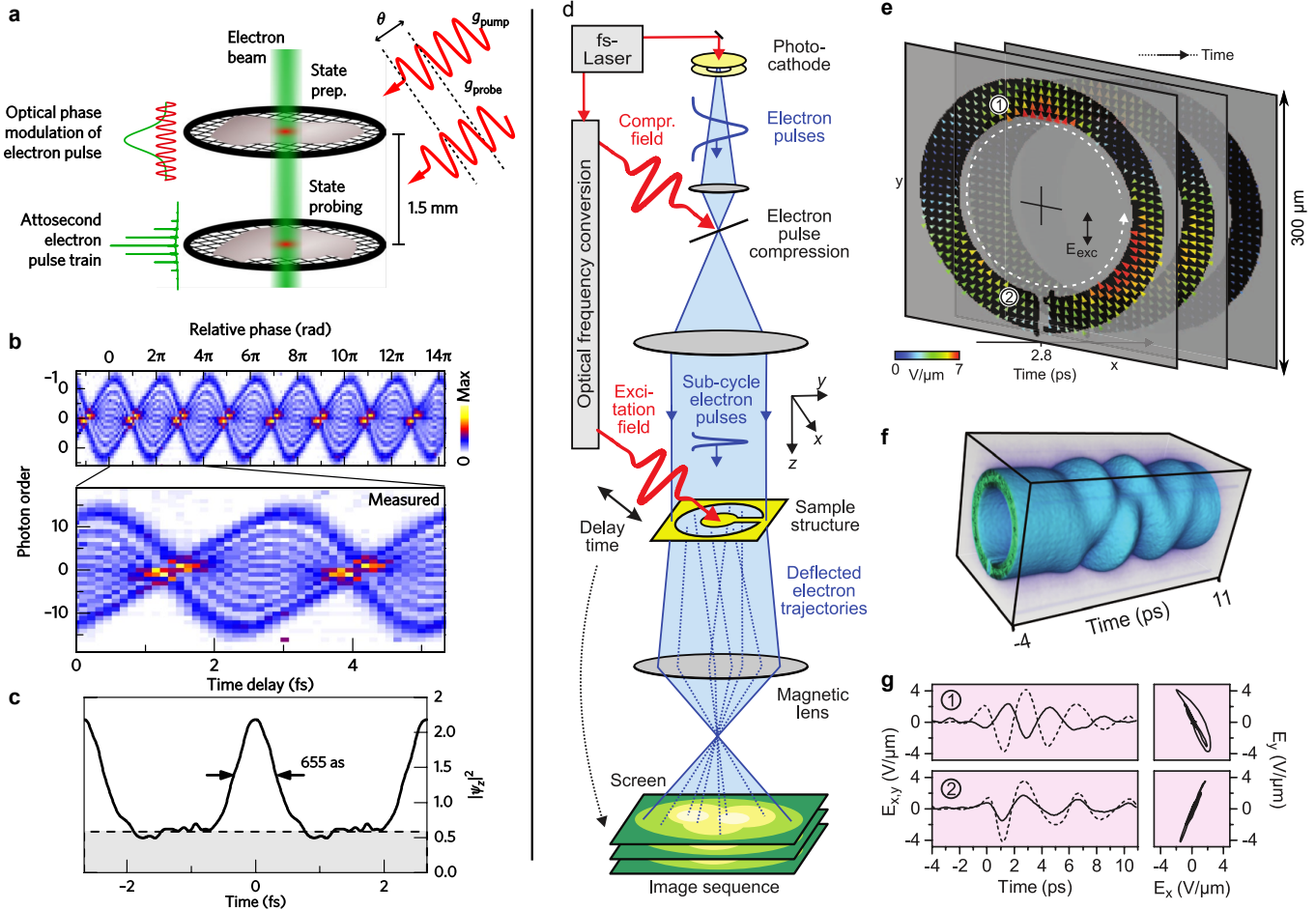


FIG. 5. Applications of ultrafast electron sources. Panels (a)-(c) show the generation and subsequent characterization of attosecond electron pulse trains [from Ref. 79]: (a) Scheme of the experimental setup for attosecond electron pulse trains generation and characterization with graphite nanofoils on upper and lower grids, respectively. Two phase-locked laser pulses of the same frequency, together with the electron beam are used to prepare and probe the attosecond electron pulse trains. (b) Measured electron kinetic energy shift (in units of the photon energy) depending on the phase-delay between preparation and probe laser pulses. (c) Reconstructed electron pulse duration. (d)-(g) Sub-cycle/sub-wavelength-resolved space-time reconstruction of THz electromagnetic field inside a microresonator [from Ref. 78]. (d) Scheme of the experimental setup: The same laser drives electron pulse generation, compression and sample excitation, leading to exceptional timing stability. (e) Reconstructed electric fields inside the microresonator at a fixed delay time. (f) Visualization of the measured time-dependent electron signal obtained from the image sequence from which the electromagnetic fields are reconstructed. (g) Time evolutions of electric field components (left) and polarizations (right) at positions 1 and 2 inside the microresonator indicated in panel (e).

layed replica of the first laser pulse and, depending on the relative phase of the two laser pulses, the sidebands are either enhanced or reduced (see panel (b)). From this the quantum state of the electron pulse, and especially its temporal duration, can be reconstructed, as shown in panel (c). In a proof-of-principle experiment, attosecond electron pulse trains have been applied to measure the relative delay of the deflectograms of Bragg diffraction spots of silicon and found a delay of around 10 as for certain spots [169]. Numerical simulations have shown that, for single isolated attosecond pulses in similar experiments, the whole charge dynamics of e.g. graphene could potentially be reconstructed [170].

Electronic dynamics in nanostructured samples can be probed by using an ultrafast laser pump-electron pulse probe experimental scheme, where the photoinduced electron dynamics is recorded with extremely high spatial resolutions. It has been shown that using a THz pulse derived from the same laser for electron generation and

sample excitation generally leads to extremely low timing jitter [166]. In point projection microscopy experiments, spatial and temporal resolutions down to tens of nanometers and 25 fs could be demonstrated [164], which allowed the measurement of photo-induced ultrafast electric currents in semi-conductor nanowires [66] or the space-charge separation on a plasmonic nanoantenna after photoemission [164]. Here, since no electron pulse compression is employed, the temporal resolution is limited by the dispersion of the electron pulse from the source to the sample. By using electron diffraction, the atomic lattice dynamics can be probed. Using a modified transmission electron microscope, without additional pulse compression, structural phase transitions associated with charge density waves [171] or the dynamics of acoustic waves in graphite films [172] could be measured with a temporal resolution of only about 1 ps. With electron pulses compression schemes that generate attosecond pulse trains, the measurement of Bragg diffraction

spots with a resolution on the order of ten attoseconds is possible [169]. Since electrons are sensitive to electromagnetic fields, ultrafast electron pulses have been used to reconstruct the local plasmonic field induced by THz light on single microresonator with sub-100 fs and few-micron resolution [78]. The setup for this experiment is shown in Fig. 5(d), consisting of the above-mentioned elements for electron pulse generation, compression and the intrinsically synchronized pump-probe scheme. The reconstructed field distribution inside the microresonator at certain time delay is shown in panel (e) together with the measured transmitted electron signal after the sample in panel (f), as well as the dynamics of the electric field components at two selected points inside the microresonator, in panel (g).

So far electron pulse durations in electron microscope setups are on the order of few tens of femtoseconds. The attosecond pulse trains, as shown above, could be used to probe periodic dynamics. However, in order to probe more complex electronic dynamics or to fully reconstruct electromagnetic fields with frequencies up to PHz scales, isolated attosecond electron pulses are needed. To achieve this, the use of compression schemes seems unavoidable. In this case, stronger THz fields would be beneficial, as well as a cascade of different compression stages with different laser frequencies. We believe that electron-pulse based techniques, thanks to their excellent spatial resolution and the well-established methodology in static modes of operation, could offer a substantial potential for both fundamental research as well as attosecond nanoscopy applications in material and surface analysis. Since they can measure both electric near-fields as well as charge dynamics, they hold the promise to also become an exceptional analytical tool in the development of light-driven peta-

hertz electronics.

## CONCLUSIONS

Thanks to the tremendous advances that have been made in the field of attosecond nanophysics over the past few years, the research is now in a position to expect several promising technological applications. In this perspective, we have discussed metrology for petahertz electronics applications including HHG and ultrafast current in nanostructured solids, as well as the development of attosecond metrology for nanoscopy, including Atto-PEEM and ultrafast electron pulses. We have pointed out the major challenges of each topics, and their avenues of further development.

## ACKNOWLEDGMENTS

J. S., Z. W., and M. F. K. acknowledge support by the Max Planck Society, the DFG via the cluster of excellence “Munich Centre for Advanced Photonics” and from the PETACOM project financed by FET Open H2020 program of the European Union. M. F. C. acknowledges the project Advanced research using high intensity laser produced photons and particles (CZ.02.1.01/0.0/0.0/16\_019/0000789) from European Regional Development Fund (ADONIS). E.P. and M.L. acknowledge the Spanish Ministry MINECO (National Plan 15 Grant: FISICATEAMO No. FIS2016-79508-P, SEVERO OCHOA No. SEV-2015-0522, FPI), European Social Fund, Fundació Cellex, Generalitat de Catalunya (AGAUR Grant No. 2017 SGR 1341 and CERCA/Program), ERC AdG OSYRIS and NOQIA, and the National Science Centre, Poland-Symfonia Grant No. 2016/20/W/ST4/00314.

- 
- [1] F. Krausz and M. I. Stockman. Attosecond metrology: from electron capture to future signal processing. *Nat. Photon.* **8** no. 3, pp. 205–213 (2014).
  - [2] E. Goulielmakis et al. Attosecond control and measurement: Lightwave electronics. *Science* **317** no. 5839, pp. 769–775 (2007).
  - [3] F. Krausz and M. Ivanov. Attosecond physics. *Rev. Mod. Phys.* **81** no. 1, pp. 163–234 (2009).
  - [4] M. Nisoli et al. Attosecond electron dynamics in molecules. *Chem. Rev.* **117** no. 16, pp. 10 760–10 825 (2017).
  - [5] I. Crassee et al. Strong field transient manipulation of electronic states and bands. *Struct. Dynam.* **6** no. 6, p. 061 505 (2017).
  - [6] E. Goulielmakis et al. Single-cycle nonlinear optics. *Science* **320** no. 5883, pp. 1614–1617 (2008).
  - [7] K. Zhao et al. Tailoring a 67 attosecond pulse through advantageous phase-mismatch. *Opt. Lett.* **37** no. 18, pp. 3891–3893 (2012).
  - [8] P. B. Corkum. Plasma perspective on strong field multi-photon ionization. *Phys. Rev. Lett.* **71** no. 13, pp. 1994–1997 (1993).
  - [9] K. C. Kulander, K. J. Schafer and J. L. Krause. Dynamics of short-pulse excitation, ionization and harmonic conversion. In B. Piraux, A. L’Huillier and K. Rzążewski (eds.), *Super-Intense Laser Atom Physics*, vol. 316 of *NATO Advanced Studies Institute Series B: Physics*, pp. 95–110 (Plenum, New York, 1993).
  - [10] M. Lewenstein et al. Theory of high-harmonic generation by low-frequency laser fields. *Phys. Rev. A* **49** no. 3, pp. 2117–2132 (1994).
  - [11] P. Salières et al. Study of spatial and temporal coherence of high order harmonics. In B. Bederson and H. Walther (eds.), *Adv. At. Mol. Opt. Phys.*, vol. 41, pp. 83–142 (Academic Press, 1999). arXiv:quant-ph/9710060.
  - [12] T. Brabec (ed.). *Strong Field Laser Physics*. Springer series in optical sciences, vol. 134 ed. (Springer-Verlag, New York, 2008).
  - [13] F. Calegari et al. Advances in attosecond science. *J. Phys. B: At. Mol. Opt. Phys.* **49** no. 6, p. 062 001 (2016).
  - [14] K. Amini et al. Symphony on strong field approximation. *Rep. Prog. Phys.* **82** no. 11, p. 116 001 (2019). arXiv:1812.11447.
  - [15] S. Ghimire et al. Strong-field and attosecond physics in solids. *J. Phys. B: At. Mol. Opt. Phys.* **47** no. 20, p. 204 030 (2014).
  - [16] A. H. Chin, O. G. Calderón and J. Kono. Extreme mid-infrared nonlinear optics in semiconductors. *Phys. Rev. Lett.* **86** no. 15, pp. 3292–3295 (2001).
  - [17] S. Ghimire et al. Observation of high-order harmonic

- generation in a bulk crystal. *Nat. Phys.* **7** no. 2, pp. 138–141 (2011).
- [18] O. Schubert et al. Sub-cycle control of terahertz high-harmonic generation by dynamical bloch oscillations. *Nat. Photon.* **8** no. 2, pp. 119–123 (2014).
- [19] T. T. Luu et al. Extreme ultraviolet high-harmonic spectroscopy of solids. *Nature* **521** no. 7553, pp. 498–502 (2015).
- [20] G. Vampa et al. Linking high harmonics from gases and solids. *Nature* **522** no. 7557, pp. 462–464 (2015).
- [21] S. Ghimire and D. A. Reis. High-harmonic generation from solids. *Nat. Phys.* **15** no. 1, pp. 10–16 (2019).
- [22] M. Schultze et al. Attosecond band-gap dynamics in silicon. *Science* **346** no. 6215, pp. 1348–1352 (2014).
- [23] F. Schlaepfer et al. Attosecond optical-field-enhanced carrier injection into the GaAs conduction band. *Nat. Phys.* **14** no. 6, pp. 560–564 (2018).
- [24] L. Seiffert et al. Attosecond chronoscopy of electron scattering in dielectric nanoparticles. *Nat. Phys.* **13** no. 8, pp. 766–770 (2017).
- [25] A. Schiffriin et al. Optical-field-induced current in dielectrics. *Nature* **493** no. 7430, pp. 70–74 (2013).
- [26] M. Schultze et al. Controlling dielectrics with the electric field of light. *Nature* **493** no. 7430, pp. 75–78 (2013).
- [27] T. Paasch-Colberg et al. Solid-state light-phase detector. *Nat. Photon.* **8** no. 3, pp. 214–218 (2014).
- [28] T. Paasch-Colberg et al. Sub-cycle optical control of current in a semiconductor: from the multiphoton to the tunneling regime. *Optica* **3** no. 12, pp. 1358–1361 (2016).
- [29] R. Silva et al. Topological strong-field physics on sub-laser-cycle timescale. *Nat. Photon.* **13** no. 12, pp. 849–854 (2019). arXiv:1806.11232.
- [30] A. Chacón et al. Observing topological phase transitions with high harmonic generation (2018). arXiv:1807.01616.
- [31] C. Jürk and D. Bauer. High-harmonic generation in Su-Schrieffer-Heeger chains. *Phys. Rev. B* **99** no. 19, p. 195428 (2019).
- [32] R. Silva et al. High-harmonic spectroscopy of ultrafast many-body dynamics in strongly correlated systems. *Nature Photon.* **12** no. 5, p. 266 (2018). arXiv:1704.08471.
- [33] V. Mourik et al. Signatures of Majorana fermions in hybrid superconductor-semiconductor nanowire devices. *Science* **336** no. 6084, pp. 1003–1007 (2012).
- [34] R. M. Lutchyn et al. Majorana zero modes in superconductor–semiconductor heterostructures. *Nat. Rev. Mat.* **3** no. 5, pp. 152–68 (2018).
- [35] D. M. van Zanten et al. Photon assisted tunneling of zero modes in a Majorana wire (2019). arXiv:1902.00797.
- [36] R. Hanson et al. Spins in few-electron quantum dots. *Rev. Mod. Phys.* **79** no. 4, pp. 1217–1265 (2007).
- [37] P. Senellart, G. Solomon and A. White. High-performance semiconductor quantum-dot single-photon sources. *Nat. Nanotech.* **12**, pp. 1026–1039 (2017).
- [38] A. Delteil et al. Realization of a cascaded quantum system: Heralded absorption of a single photon qubit by a single-electron charged quantum dot. *Phys. Rev. Lett.* **118** no. 17, p. 177401 (2017).
- [39] J. R. Schaibley et al. Valleytronics in 2D materials. *Nat. Rev. Mat.* **1**, p. 16055 (2016).
- [40] Y. Cao et al. Unconventional superconductivity in magic-angle graphene superlattices. *Nature* **556**, pp. 43–50 (2018).
- [41] M. Z. Hasan and C. L. Kane. Colloquium: Topological insulators. *Rev. Mod. Phys.* **82**, pp. 3045–3067 (2010).
- [42] S.-Y. Xu et al. Electrically switchable Berry curvature dipole in the monolayer topological insulator WTe<sub>2</sub>. *Nat. Phys.* **14**, pp. 900–906 (2018).
- [43] P. Hommelhoff and M. F. Kling. *Attosecond Nanophysics: From Basic Science to Applications* (Wiley-VCH, Weinheim, 2015).
- [44] M. F. Ciappina et al. Attosecond physics at the nanoscale. *Rep. Prog. Phys.* **80** no. 5, p. 054401 (2017).
- [45] B. Förg et al. Attosecond nanoscale near-field sampling. *Nat. Commun.* **7**, p. 11717 (2017).
- [46] M. F. Ciappina et al. Above-threshold ionization by few-cycle spatially inhomogeneous fields. *Phys. Rev. A* **86** no. 2, p. 023413 (2012).
- [47] M. F. Ciappina et al. Electron-momentum distributions and photoelectron spectra of atoms driven by an intense spatially inhomogeneous field. *Phys. Rev. A* **87** no. 6, p. 063833 (2013).
- [48] J. A. Pérez-Hernández et al. Beyond carbon K-edge harmonic emission using a spatial and temporal synthesized laser field. *Phys. Rev. A* **110** no. 5, p. 053001 (2013).
- [49] A. Fleischer et al. Spin angular momentum and tunable polarization in high-harmonic generation. *Nat. Photon.* **8** no. 7, pp. 543–549 (2014).
- [50] E. Pisanty et al. Knotting fractional-order knots with the polarization state of light. *Nat. Photon.* **13**, pp. 569–574 (2019).
- [51] O. Kfir et al. Generation of bright phase-matched circularly-polarized extreme ultraviolet high harmonics. *Nat. Photon.* **9**, pp. 99–105 (2015).
- [52] E. Pisanty et al. Conservation of torus-knot angular momentum in high-order harmonic generation. *Phys. Rev. Lett.* **122** no. 20, p. 203201 (2019).
- [53] L. Rego et al. Generation of extreme-ultraviolet beams with time-varying orbital angular momentum. *Science* **364** no. 6447, p. eaaw9486 (2019).
- [54] D. Ayuso et al. Locally and globally chiral fields for ultimate control of chiral light matter interaction (2018). arXiv:1809.01632.
- [55] P. Hommelhoff et al. Field emission tip as a nanometer source of free electron femtosecond pulses. *Phys. Rev. Lett.* **96** no. 7, p. 077401 (2006).
- [56] P. Hommelhoff, C. Kealhofer and M. A. Kasevich. Ultrafast electron pulses from a tungsten tip triggered by low-power femtosecond laser pulses. *Phys. Rev. Lett.* **97** no. 24, p. 247402 (2006).
- [57] C. Ropers et al. Localized multiphoton emission of femtosecond electron pulses from metal nanotips. *Phys. Rev. Lett.* **98** no. 4, p. 043907 (2007).
- [58] B. Barwick et al. Laser-induced ultrafast electron emission from a field emission tip. *New J. Phys.* **9** no. 5, p. 142 (2007).
- [59] M. I. Stockman et al. Attosecond nanoplasmonic-field microscope. *Nat. Photon.* **1** no. 9, pp. 539–544 (2007).
- [60] M. Schenk, M. Krüger and P. Hommelhoff. Strong-field above-threshold photoemission from sharp metal tips. *Phys. Rev. Lett.* **105** no. 25, p. 257601 (2010).
- [61] R. Bormann et al. Tip-enhanced strong-field photoemission. *Phys. Rev. Lett.* **105** no. 14, p. 147601 (2010).
- [62] S. Zherebtsov et al. Controlled near-field enhanced electron acceleration from dielectric nanospheres with intense few-cycle laser fields. *Nat. Phys.* **7** no. 8, pp. 656–662 (2011).
- [63] M. Krüger, M. Schenk and P. Hommelhoff. Attosecond control of electrons emitted from a nanoscale metal tip. *Nature* **475** no. 7354, pp. 78–81 (2011).
- [64] B. Piglosiewicz et al. Carrier-envelope phase effects on the strong-field photoemission of electrons from metallic nanostructures. *Nat. Photon.* **8** no. 1, pp. 37–42 (2014).
- [65] M. Gulde et al. Ultrafast low-energy electron diffraction in transmission resolves polymer/graphene superstructure dynamics. *Science* **345** no. 6193, pp. 200–204 (2014).
- [66] M. Müller, A. Paarmann and R. Ernststorfer. Femtosec-

- ond electrons probing currents and atomic structure in nanomaterials. *Nat. Commun.* **5**, p. 5292 (2014).
- [67] D. Ehberger et al. Highly coherent electron beam from a laser-triggered tungsten needle tip. *Phys. Rev. Lett.* **114** no. 22, p. 227601 (2015).
- [68] J. Vogelsang et al. Plasmonic-nanofocusing-based electron holography. *ACS Photonics* **5** no. 9, pp. 3584–3595 (2018).
- [69] T. Higuchi et al. A nanoscale vacuum-tube diode triggered by few-cycle laser pulses. *Appl. Phys. Lett.* **106** no. 5, p. 051109 (2015).
- [70] D. Hoff et al. Tracing the phase of focused broadband laser pulses. *Nat. Phys.* **13** no. 10, pp. 947–951 (2017).
- [71] H. Liu et al. High-harmonic generation from an atomically thin semiconductor. *Nat. Phys.* **13** no. 3, pp. 262–265 (2017).
- [72] N. Yoshikawa, T. Tamaya and K. Tanaka. High-harmonic generation in graphene enhanced by elliptically polarized light excitation. *Science* **356** no. 6339, pp. 736–738 (2017).
- [73] S. Han et al. High-harmonic generation by field enhanced femtosecond pulses in metal-sapphire nanostructure. *Nat. Commun.* **7**, p. 13105 (2016).
- [74] M. Sivis et al. Tailored semiconductors for high-harmonic optoelectronics. *Science* **357** no. 6348, pp. 303–306 (2017).
- [75] T. Higuchi et al. Light-field-driven currents in graphene. *Nature* **550** no. 7675, pp. 224–228 (2017).
- [76] J. Itatani et al. Attosecond streak camera. *Phys. Rev. Lett.* **88** no. 17, p. 173903 (2002).
- [77] R. Kienberger et al. Atomic transient recorder. *Nature* **427** no. 6977, pp. 817–821 (2004).
- [78] A. Ryabov and P. Baum. Electron microscopy of electromagnetic waveforms. *Science* **353** no. 6297, pp. 374–377 (2016).
- [79] K. E. Priebe et al. Attosecond electron pulse trains and quantum state reconstruction in ultrafast transmission electron microscopy. *Nat. Photon.* **11** no. 12, pp. 793–797 (2017).
- [80] G. Vampa et al. Plasmon-enhanced high-harmonic generation from silicon. *Nat. Phys.* **13** no. 7, pp. 659–662 (2017).
- [81] S. Kim et al. High-harmonic generation by resonant plasmon field enhancement. *Nature* **453** no. 7196, pp. 757–760 (2008).
- [82] I.-Y. Park et al. Plasmonic generation of ultrashort extreme-ultraviolet light pulses. *Nat. Photon.* **5** no. 11, pp. 677–681 (2011).
- [83] M. Sivis et al. Nanostructure-enhanced atomic line emission. *Nature* **485** no. 7397, pp. E1–E3 (2012).
- [84] M. Sivis et al. Extreme-ultraviolet light generation in plasmonic nanostructures. *Nat. Phys.* **9** no. 5, pp. 304–309 (2013).
- [85] M. B. Raschke. High-harmonic generation with plasmonics: feasible or unphysical?. *Ann. Phys. (Berlin)* **525** no. 3, pp. A40–A42 (2013).
- [86] G. Vampa and T. Brabec. Merge of high harmonic generation from gases and solids and its implications for attosecond science. *J. Phys. B: At., Mol. Opt. Phys.* **50** no. 8, p. 083001 (2017).
- [87] S. Y. Kruchinin, F. Krausz and V. S. Yakovlev. Colloquium: Strong-field phenomena in periodic systems. *Rev. Mod. Phys.* **90** no. 2, p. 021002 (2018).
- [88] U. Huttner, M. Kira and S. W. Koch. Ultrahigh off-resonant field effects in semiconductors. *Laser Phot. Rev.* **11** no. 4, p. 1700049 (2017).
- [89] R. A. Ganeev et al. Effective high-order harmonic generation from metal sulfide quantum dots. *Opt. Exp.* **26** no. 26, pp. 35013–35025 (2018).
- [90] H. Liu et al. Enhanced high-harmonic generation from an all-dielectric metasurface. *Nat. Phys.* **14** no. 10, pp. 1006–1010 (2018).
- [91] M. Timofeeva et al. Anapoles in free-standing III $\text{AsV}$  nanodisks enhancing second-harmonic generation. *Nano Lett.* **18** no. 6, pp. 3695–3702 (2018).
- [92] A. Fleischer et al. Spin angular momentum and tunable polarization in high-harmonic generation. *Nat. Photon.* **8** no. 7, pp. 543–549 (2014).
- [93] D. Azoury et al. Interferometric attosecond lock-in measurement of extreme-ultraviolet circular dichroism. *Nat. Photon.* **13** no. 3, pp. 198–204 (2019).
- [94] D. Gauthier et al. Tunable orbital angular momentum in high-harmonic generation. *Nat. Commun.* **8**, p. 14971 (2017).
- [95] K. M. Dorney et al. Controlling the polarization and vortex charge of attosecond high-harmonic beams via simultaneous spin-orbit momentum conservation. *Nat. Photon.* **13** no. 2, pp. 123–130 (2019).
- [96] D. Gauthier et al. Orbital angular momentum from semiconductor high-order harmonics. *Opt. Lett.* **44** no. 3, pp. 546–549 (2019).
- [97] N. Pfullmann et al. Bow-tie nano-antenna assisted generation of extreme ultraviolet radiation. *New J. Phys.* **15** no. 9, p. 093027 (2013).
- [98] L. Liu et al. Highly localized heat generation by femtosecond laser induced plasmon excitation in ag nanowires. *Appl. Phys. Lett.* **102** no. 7, p. 073107 (2013).
- [99] A. M. Summers et al. Optical damage threshold of au nanowires in strong femtosecond laser fields. *Opt. Exp.* **22** no. 4, pp. 4235–4246 (2014).
- [100] C. Homann et al. Carrier-envelope phase stable sub-two-cycle pulses tunable around 1.8  $\mu\text{m}$  at 100 khz. *Opt. Lett.* **37** no. 10, pp. 1673–1675 (2012).
- [101] H. Fattahi et al. Third-generation femtosecond technology. *Optica* **1** no. 1, pp. 45–63 (2014).
- [102] H. Liang et al. High-energy mid-infrared sub-cycle pulse synthesis from a parametric amplifier. *Nat. Commun.* **8**, p. 141 (2017).
- [103] M. Neuhaus et al. 10 W CEP-stable few-cycle source at 2  $\mu\text{m}$  with 100 kHz repetition rate. *Opt. Exp.* **26** no. 13, pp. 16074–16085 (2018).
- [104] F. Lu et al. Generation of sub-two-cycle cep-stable optical pulses at 3.5  $\mu\text{m}$  from a kta-based optical parametric amplifier with multiple-plate compression. *Opt. Lett.* **43** no. 11, pp. 2720–2723 (2018).
- [105] T. Rybka et al. Sub-cycle optical phase control of nanotunnelling in the single-electron regime. *Nat. Photon.* **10** no. 10, pp. 667–670 (2016).
- [106] W. P. Putnam et al. Optical-field-controlled photoemission from plasmonic nanoparticles. *Nat. Phys.* **13** no. 4, pp. 335–339 (2017).
- [107] S. E. Irvine and A. Y. Elezzabi. Ponderomotive electron acceleration using surface plasmon waves excited with femtosecond laser pulses. *Appl. Phys. Lett.* **86** no. 26, p. 264102 (2005).
- [108] P. Dombi et al. Observation of few-cycle, strong-field phenomena in surface plasmon fields. *Opt. Exp.* **18** no. 23, pp. 24206–24212 (2010).
- [109] P. Rácz et al. Strong-field plasmonic electron acceleration with few-cycle, phase-stabilized laser pulses. *Appl. Phys. Lett.* **98** no. 11, p. 111116 (2011).
- [110] O. Kwon et al. Semimetalization of dielectrics in strong optical fields. *Sci. Rep.* **6**, p. 21272 (2016).
- [111] O. Kwon and D. Kim. Phz current switching in calcium fluoride single crystal. *Appl. Phys. Lett.* **108** no. 19, p. 191112 (2016).
- [112] J. D. Lee, W. S. Yun and N. Park. Rectifying the optical-field-induced current in dielectrics: Petahertz diode. *Phys. Rev. Lett.* **116** no. 5, p. 057401 (2016).

- [113] J. D. Lee, Y. Kim and C.-M. Kim. Model for petahertz optical memory based on a manipulation of the optical-field-induced current in dielectrics. *New J. Phys.* **20** no. 9, p. 093 029 (2018).
- [114] M. Garg et al. Multi-petahertz electronic metrology. *Nature* **538**, pp. 359–363 (2016).
- [115] A. Sommer et al. Attosecond nonlinear polarization and light-matter energy transfer in solids. *Nature* **534** no. 7605, pp. 86–90 (2016).
- [116] H. Mashiko et al. Petahertz optical drive with wide-bandgap semiconductor. *Nat. Phys.* **12**, pp. 741–745 (2016).
- [117] M. I. Stockman. Nanofocusing of optical energy in tapered plasmonic waveguides. *Phys. Rev. Lett.* **93** no. 13, p. 137 404 (2004).
- [118] C. C. Neacsu et al. Near-field localization in plasmonic superfocusing: a nanoemitter on a tip. *Nano Lett.* **10** no. 2, pp. 592–596 (2010).
- [119] S. Berweger et al. Adiabatic tip-plasmon focusing for nano-raman spectroscopy. *J. Phys. Chem. Lett.* **1** no. 24, pp. 3427–3432 (2010).
- [120] F. D. Angelis et al. Breaking the diffusion limit with super-hydrophobic delivery of molecules to plasmonic nanofocusing sers structures. *Nat. Photon.* **5** no. 11, p. 682 (2011).
- [121] S. Schmidt et al. Adiabatic nanofocusing on ultrasmooth single-crystalline gold tapers creates a 10-nm-sized light source with few-cycle time resolution. *ACS Nano* **6** no. 7, pp. 6040–6048 (2012).
- [122] A. Hugi et al. Mid-infrared frequency comb based on a quantum cascade laser. *Nature* **492** no. 7428, pp. 229–233 (2012).
- [123] F. Wang et al. Generating ultrafast pulses of light from quantum cascade lasers. *Optica* **2** no. 11, pp. 944–949 (2015).
- [124] A. Mottaghizadeh et al. 5-ps-long terahertz pulses from an active-mode-locked quantum cascade laser. *Optica* **4** no. 1, pp. 168–171 (2017).
- [125] T. J. Kippenberg et al. Dissipative Kerr solitons in optical microresonators. *Science* **361** no. 6402, p. eaan8083 (2018).
- [126] A. Pasquazi et al. Micro-combs: a novel generation of optical sources. *Phys. Rep.* **729**, pp. 1–81 (2018).
- [127] J. Pfeifle et al. Coherent terabit communications with microresonator Kerr frequency combs. *Nat. Photon.* **8** no. 5, pp. 375–380 (2014).
- [128] M. L. Weichman et al. Broadband molecular spectroscopy with optical frequency combs. *J. Mol. Spectrosc.* **355**, pp. 66–78 (2019).
- [129] N. Picqué and T. W. Hänsch. Frequency comb spectroscopy. *Nat. Photon.* **13**, pp. 146–157 (2019).
- [130] B. Stern et al. Battery-operated integrated frequency comb generator. *Nature* **562**, pp. 401–405 (2018).
- [131] S. H. Chew et al. Time-of-flight-photoelectron emission microscopy on plasmonic structures using attosecond extreme ultraviolet pulses. *Appl. Phys. Lett.* **100** no. 5, p. 051 904 (2012).
- [132] T. Saule et al. High-flux ultrafast extreme-ultraviolet photoemission spectroscopy at 18.4 MHz pulse repetition rate. *Nat. Commun.* **10**, p. 458 (2019).
- [133] C.-T. Chiang et al. Boosting laboratory photoelectron spectroscopy by megahertz high-order harmonics. *New J. Phys.* **17** no. 1, p. 013 035 (2015).
- [134] B. Frietsch et al. A high-order harmonic generation apparatus for time-and angle-resolved photoelectron spectroscopy. *Rev. Sci. Instrum.* **84** no. 7, p. 075 106 (2013).
- [135] A. Mikkelsen et al. Photoemission electron microscopy using extreme ultraviolet attosecond pulse trains. *Rev. Sci. Instrum.* **80** no. 12, p. 123 703 (2009).
- [136] G. L. Dakovski et al. Tunable ultrafast extreme ultraviolet source for time-and angle-resolved photoemission spectroscopy. *Rev. Sci. Instrum.* **81** no. 7, p. 073 108 (2010).
- [137] C. Corder et al. Ultrafast extreme ultraviolet photoemission without space charge. *Struct. Dyn.* **5** no. 5, p. 054 301 (2018).
- [138] A. K. Mills et al. An XUV source using a femtosecond enhancement cavity for photoemission spectroscopy. In S. G. Biedron (ed.), *Proc. SPIE 9512, Advances in X-ray Free-Electron Lasers Instrumentation III* (SPIE, 2015), p. 95121I.
- [139] M. I. Stockman et al. Roadmap on plasmonics. *J. of Opt.* **20** no. 4, p. 043 001 (2018).
- [140] E. Skopalová et al. Numerical simulation of attosecond nanoplasmonic streaking. *New J. Phys.* **13** no. 8, p. 083 003 (2011).
- [141] F. Süßmann and M. F. Kling. Attosecond nanoplasmonic streaking of localized fields near metal nanospheres. *Phys. Rev. B* **84** no. 12, p. 121 406 (2011).
- [142] A. G. Borisov, P. M. Echenique and A. K. Kazansky. Attostreaking with metallic nano-objects. *New J. Phys.* **14** no. 2, p. 023 036 (2012).
- [143] F. Kelkensberg, A. F. Koenderink and M. J. J. Vrakking. Attosecond streaking in a nano-plasmonic field. *New J. Phys.* **14** no. 9, p. 093 034 (2012).
- [144] J. S. Prell et al. Simulation of attosecond-resolved imaging of the plasmon electric field in metallic nanoparticles. *Ann. Phys. (Berlin)* **525** no. 1-2, pp. 151–161 (2013).
- [145] M. Lupetti et al. Attosecond photocopy of plasmonic excitations. *Phys. Rev. Lett.* **113** no. 11, p. 113 903 (2014).
- [146] J. Li, E. Saydanzad and U. Thumm. Imaging plasmonic fields near au nanospheres with spatiotemporal resolution. *Phys. Rev. Lett.* **120** no. 22, p. 223 903 (2018).
- [147] E. Goulielmakis et al. Direct measurement of light waves. *Science* **305** no. 5688, pp. 1267–1269 (2004).
- [148] J. Schötz et al. Reconstruction of nanoscale near fields by attosecond streaking. *IEEE J. Sel. Top. Quant.* **23** no. 3, pp. 77–87 (2017).
- [149] Z. Tao et al. Direct time-domain observation of attosecond final-state lifetimes in photoemission from solids. *Science* **353** no. 6294, pp. 62–67 (2016).
- [150] S. Eich et al. Time-and angle-resolved photoemission spectroscopy with optimized high-harmonic pulses using frequency-doubled Ti:Sapphire lasers. *J. Electron Spectrosc.* **195**, pp. 231–236 (2014).
- [151] A. Cingöz et al. Direct frequency comb spectroscopy in the extreme ultraviolet. *Nature* **482** no. 7383, pp. 68–71 (2012).
- [152] I. Pupeza et al. Compact high-repetition-rate source of coherent 100 eV radiation. *Nat. Photon.* **7** no. 8, pp. 608–612 (2013).
- [153] C. Corder et al. An instrument for time-resolved photo-electron spectroscopy at 87 mhz. In *Frontiers in Optics 2017* (Optical Society of America, 2017), p. LM4F.6.
- [154] A. Ozawa et al. High average power coherent VUV generation at 10 MHz repetition frequency by intracavity high harmonic generation. *Opt. Exp.* **23** no. 12, pp. 15 107–15 118 (2015).
- [155] G. Porat et al. Phase-matched extreme-ultraviolet frequency-comb generation. *Nat. Photon.* **12** no. 7, pp. 387–391 (2018).
- [156] A. Vernaleken et al. Single-pass high-harmonic generation at 20.8 MHz repetition rate. *Opt. Lett.* **36** no. 17, pp. 3428–3430 (2011).
- [157] S. Hädrich et al. Single-pass high harmonic generation at high repetition rate and photon flux. *J. Phys. B: At. Mol. Opt. Phys.* **49** no. 17, p. 172 002 (2016).
- [158] J. Rothhardt et al. High average power near-infrared

- few-cycle lasers. *Laser Phot. Rev.* **11** no. 4, p. 1700 043 (2017).
- [159] N. Lilienfein et al. Enhancement cavities for few-cycle pulses. *Opt. Lett.* **42** no. 2, pp. 271–274 (2017).
- [160] M. Högner, V. Tosa and I. Pupeza. Generation of isolated attosecond pulses with enhancement cavities—a theoretical study. *New J. Phys.* **19** no. 3, p. 033 040 (2017).
- [161] J. Rothhardt et al. Thermal effects in high average power optical parametric amplifiers. *Opt. Lett.* **38** no. 5, pp. 763–765 (2013).
- [162] S. Hädrich et al. Scalability of components for kW-level average power few-cycle lasers. *Appl. Opt.* **55** no. 7, pp. 1636–1640 (2016).
- [163] M. Krebs et al. Towards isolated attosecond pulses at megahertz repetition rates. *Nat. Photon.* **7** no. 7, pp. 555–559 (2013).
- [164] J. Vogelsang et al. Observing charge separation in nanoantennas via ultrafast point-projection electron. *Light Sci. Appl.* **7** no. 1, p. 55 (2018).
- [165] A. Feist et al. Structural dynamics probed by high-coherence electron pulses. *MRS Bulletin* **43** no. 7, pp. 504–511 (2018).
- [166] C. Kealhofer et al. All-optical control and metrology of electron pulses. *Science* **352** no. 6284, pp. 429–433 (2016).
- [167] Y. Morimoto and P. Baum. Attosecond control of electron beams at dielectric and absorbing membranes. *Phys. Rev. A* **97** no. 3, p. 033 815 (2018).
- [168] F. O. Kirchner et al. Laser streaking of free electrons at 25 keV. *Nat. Photon.* **8** no. 1, pp. 52–57 (2014).
- [169] Y. Morimoto and P. Baum. Diffraction and microscopy with attosecond electron pulse trains. *Nat. Phys.* **14** no. 3, pp. 252–256 (2018).
- [170] V. S. Yakovlev et al. Atomic-scale diffractive imaging of sub-cycle electron dynamics in condensed matter. *Sci. Rep.* **5**, p. 14 581 (2015).
- [171] S. Vogelgesang et al. Phase ordering of charge density waves traced by ultrafast low-energy electron diffraction. *Nat. Photon.* **14** no. 2, pp. 184–190 (2018).
- [172] A. Feist et al. Nanoscale diffractive probing of strain dynamics in ultrafast transmission electron microscopy. *Struct. Dynam.* **5** no. 1, p. 014 302 (2018).